Published in final edited form as:

Pediatr Res. 2020 September ; 88(3): 382–390. doi:10.1038/s41390-020-0788-7.

Increased rates of vesicoureteral reflux in mice from deletion of *Dicer* in the peri-Wolffian duct stroma

Melissa J. Anslow[1,2,*], **Andrew J. Bodnar**[1,2], **Débora M. Cerqueira**[1,2], **Daniel Bushnell**[1,2], **Brynn E. Shrom**[1,3], **Sunder Sims-Lucas**[1,2], **Carlton M. Bates**[1,2], **Jacqueline Ho**[1,2]

[1]Rangos Research Center, Children's Hospital of Pittsburgh of UPMC, Pittsburgh, PA

[2]Department of Pediatrics, Division of Nephrology, University of Pittsburgh School of Medicine, PA

[3]Missouri University of Science and Technology, Rolla, MO

Abstract

BACKGROUND: Vesicoureteral reflux (VUR), backflow of urine into the kidney, is associated with urinary tract infections and chronic kidney disease. Integrity of the vesicoureteral junction (VUJ), where reflux occurs, is determined largely by proper induction of the ureteric bud from the Wolffian duct. Induction is modulated by signals from the surrounding peri-Wolffian duct stroma. We evaluated whether miRNAs in the peri-Wolffian duct stroma are necessary for proper ureteric induction, VUJ formation, and suppression of VUR.

METHODS: We generated a mouse with loss of miRNAs in the peri-Wolffian duct stroma. We evaluated embryos for ureteric bud induction defects and expression of genes that regulate induction. We performed cystograms to assess for reflux and assessed VUJs in postnatal mice.

RESULTS: Mutant embryos had cranially displaced ureteric bud induction sites versus controls. We observed no changes in expression of genes known to regulate induction. While mutants were early postnatal lethal, they had high rates of VUR versus controls. Mutant VUJs that refluxed had low inserting ureters and shortened intravesicular tunnels versus non-refluxing mice.

CONCLUSIONS: We found that miRNAs in the peri-Wolffian duct stroma are required for normal ureteric bud induction, VUJ formation, and prevention of VUR.

Introduction

Vesicoureteral reflux (VUR), abnormal backflow of urine from the bladder to the kidneys, is a congenital urinary tract abnormality that is reported in 1-2% of the general population and in 30-50% of patients with urinary tract infection [1, 2]. VUR is associated with

[*]**Corresponding author:** Dr. Melissa Anslow, Rangos Research Center, Children's Hospital of Pittsburgh of UPMC, 4401 Penn Ave, Pittsburgh, Pennsylvania 1522441, USA, Phone: 412-692-7808, melissa.anslow@chp.edu.

Author Involvement: JH and CB were involved in manuscript draft revisions. All authors contributed to experimental design and/or data collection and approved the manuscript prior to submission.

Disclosure Statement: The authors have no disclosures.

Category of Study: Basic Science

hypertension and reflux nephropathy. Reflux nephropathy is a common cause of end-stage renal disease in children. Medical and/or surgical treatment of VUR has not decreased the incidence of reflux nephropathy in the past 40 years [3].

VUR is associated with abnormal formation of the vesicoureteral junction (VUJ), including alterations in the site of ureteral insertion into the bladder and shortened intravesicular tunnel lengths (the length of ureter within the bladder wall) [4]. The site of ureter insertion into the bladder is dependent on where the ureteric bud evaginates from the Wolffian duct and physiological apoptosis of the common nephric duct, the segment of the Wolffian duct between the base of the ureteric bud and cloaca [5-7].

Ureteric bud induction from the Wolffian duct results from signals between the metanephric mesenchyme and the peri-Wolffian duct stroma (which lies between the Wolffian duct and metanephric mesenchyme) [6, 8]. Glial cell line-derived neurotrophic factor (GDNF) causes ureteric bud evagination from the duct [9]. Factors expressed in the peri-Wolffian duct stroma such as Bone morphogenetic protein 4 (*Bmp4)*, fibroblast growth factor receptor 2 (*Fgfr2*), forkhead box c1 (*Foxc1)*, and forkhead box c2 (*Foxc2)* repress ureteric induction, constraining the site to its proper position. Genetic mouse studies showed that loss of *Bmp4* [10], Gremlin 1 (*Grem1*) [8], and *Foxc1/c2* [11] lead to ureteric bud induction abnormalities. Deletion of *Fgfr2* in peri-Wolffian duct stroma led to ectopic ureteric induction sites and high rates of VUR [12]. Loss of genes in the Wolffian duct itself such as *Ret* (encoding for the GDNF receptor) and paired box gene 2 (*Pax2*) result in abnormal ureteric bud position and VUR [13,14]. Thus, many genes have been identified as suppressing VUR.

Although mouse models have identified gene mutations that cause ureteric bud defects and VUR, the genetics of human VUR is still unclear [15, 16]. Multiple inheritance patterns are described for human VUR [1]. Mutations in *BMP4*, *RET* and *PAX2* have been linked to VUR in isolated families [17, 18]. However, identification of a likely causative mutation in one family is not usually found in other families, and many families with dominant VUR inheritance have no identified gene mutations [1, 15, 16]. This raises the question of whether inherited defects in epigenetic modifiers such as noncoding RNAs might cause VUR.

MicroRNAs (miRNAs) are small, noncoding RNAs that bind to and repress expression of their target mRNAs [See [19] for a recent review]. *Dicer* is an RNaseIII enzyme that is required for processing precursor miRNAs into mature, double-stranded miRNAs [19]. Polymorphisms or differential expression of miRNAs have been associated with VUR in some patients [20-22]. However, a causative role for miRNA mutations/variations for VUR has not been established.

In this study, we examined whether miRNAs in the peri-Wolffian duct stroma are critical for prevention of VUR. Deletion of *Dicer* in the peri-Wolffian duct stroma led to cranial displacement of ureteric bud induction sites compared to littermate controls. Ureteric bud induction ectopia was not due to abnormal position of the metanephric mesenchyme, abnormal common nephric duct apoptosis, or differential expression of genes known to regulate ureteric bud induction compared to controls. Early postnatal mutants had high rates of VUR versus controls. Mutant VUJs that refluxed had lower ureter insertions into the

bladder and shorter intravesicular tunnel lengths than in non-refluxing mutant or control VUJs. Thus, miRNAs in the peri-Wolffian duct stroma are required to prevent cranial displacement of ureteric bud induction sites to allow for normal VUJ formation and suppression of VUR.

Methods

Mouse Strains

Tbx18Cre$^{Tg/+}$ mice that drive Cre recombinase expression in the peri-Wolffian duct stroma (gift from Feng Chen) [23] were bred with *Dicer*$^{flx/flx}$ mice ([24], Jackson Laboratories, Strain #00601, Bar Harbor, ME) to generate conditional knockout mice with loss of Dicer in the Tbx18-expressing lineages. *Tbx18Cre*$^{Tg/+}$*;Dicer*$^{flx/flx}$ (mutant mice) were compared to littermates without the *Tbx18Cre* allele (controls). To detect Cre expression, *Tbx18Cre*$^{Tg/+}$ mice were bred with *Gt(ROSA)26Sor*$^{tm9(CAG\text{-}tdTomato)hZE}$ (CAG) mice ([25], Jackson Laboratories, Strain #007909) to generate *Tbx18Cre*$^{Tg/+}$ *CAG* offspring in which tdTomato fluorescence is expressed in lineages arising from Tbx18Cre-positive cells. Timed matings were performed; the morning a plug was observed was considered embryonic day 0.5. We detected red fluorescence from tdTomato positive mice with a Leica M165FC Stereo Microscope (Leica, Buffalo Grove, IL). DNA was isolated from tail clippings or embryonic tissue to perform polymerase chain reaction (PCR) genotyping. All animal experiments were carried out in accordance with the policies of the Institutional Animal Care and Use Committee at the University of Pittsburgh School of Medicine (Protocol #17091432). Animals were housed in the vivarium at Rangos Research Center at the UPMC Children's Hospital of Pittsburgh, Pittsburgh, Pennsylvania.

Real-time quantitative PCR

Total RNA was isolated using the microRNeasy Micro Kit (Qiagen, Valencia, CA, USA). cDNA was synthesized using the SuperScript III First-Strand Synthesis System (Thermo Fisher Scientific, Waltham, MA, USA) using the manufacturer's protocol. Real-time quantitative PCR (qPCR) was performed with SYBR Green Master Mix (Thermo Fisher Scientific) in a 96-well C100 Thermal Cycler (Bio-Rad, Hercules, CA, USA). The expression of *Dicer* exon 24, *Dicer* exon 21, *Gdnf*, *Bmp4*, *Fgfr2*, *Grem1*, *Foxc1*, *Foxc2*, *Pax2*, and *Ret* were assessed and normalized to endogenous controls, *GAPDH* or *18S RNA*, using the cycle threshold value (C_t). Data were analyzed by the $2^{-\Delta\Delta Ct}$ method [26]. Primer sequences can be found in Supplemental Table 1 (Table S1).

Whole Mount Immunofluorescence

Embryos at E11.5 were dissected and urogenital ridges ventral to the hindlimb were exposed. Tissues were dehydrated through a methanol series and stored at −20°C. Tissues were rehydrated through a methanol series and washed with phosphate-buffered saline (PBS) with 0.1% Tween20 (PBST) three times for 10 minutes. Tissues were blocked with 10% fetal bovine serum (FBS) in PBST for one hour. Samples were incubated with primary antibody at 4°C overnight. Primary antibodies used were mouse monoclonal anti-Calbindin-D-28K (Sigma-Aldrich, 1:100, St. Louis, MO) and rabbit polyclonal anti-cleaved Caspase-3 (Cell Signaling Technology, 1:250, Danvers, MA). The tissues were washed with PBST five

times, for one hour each, then incubated overnight at 4°C with secondary antibodies, including 488 nm conjugated donkey anti-mouse IgG (Jackson ImmunoResearch, 1:250, West Grove, PA) and 594 nm conjugated goat anti-rabbit IgG (Thermo Fisher Scientific, 1:250). Tissues were washed with PBST five times, for one hour, and visualized under Leica M165FC Stereo Microscope and photographed with a QImaging Qiacam Fast 1394 camera, using QCapture software (QImaging, Surrey, BC, Canada). Common nephric duct length (caudal end of the Wolffian duct at the cloaca to the cranial edge of the ureteric bud stalk) was measured using ImageJ software (National Institutes of Health, Bethesda, MD) [27].

Histology and Immunohistochemistry

The lower body of postnatal day 0 (P0) or E11.5 mice were fixed overnight in 4% paraformaldehyde, paraffin-embedded, and sectioned at 6 μm for hematoxylin and eosin (H&E) staining or immunohistochemistry. For immunohistochemistry, tissues were deparaffinized and rehydrated. Antigen retrieval was performed by boiling the sections in 0.1 M sodium citrate buffer for 30 minutes. Samples were blocked for 30 minutes in PBST with 10% FBS. Sections were incubated with primary antibody overnight at 4°C. The primary antibodies used were mouse monoclonal anti-E-cadherin (BD Biosciences, 1:100, Franklin Lakes, NJ), mouse monoclonal calbindin-D-28K antibody (Sigma-Aldrich, 1:100), rabbit polyclonal cleaved caspase-3 antibody (Cell Signaling Technology, 1:100), and/or mouse monoclonal alpha smooth muscle actin antibody (Thermo Fisher Scientific, 1:100). Sections were washed with PBS and incubated at 4°C overnight with secondary antibodies, 488 nm conjugated donkey anti-mouse IgG (Jackson ImmunoResearch, 1:250) and/or 594 nm conjugated goat anti-rabbit IgG (Thermo Fisher Scientific, 1:250). Sections were visualized using a Leica DM 2500 light and fluorescent microscope and photographed with Leica DFC7000T camera, using Leica Application Suite X software.

3-Dimensional (3D) Reconstructions

To calculate common nephric duct length and position of the metanephric mesenchyme, E11.5 embryos embedded in paraffin were serially sectioned at 6 μm and H&E stained. The common nephric duct, ureteric bud, metanephric mesenchyme, and body wall were traced in serial sections and 3D images rendered using Stereo Investigator (MBF Bioscience, Williston, VT). The common nephric duct lengths (from the cloaca to the base of the ureteric bud) and metanephric mesenchyme volumes and positions relative to the hind limb buds were determined using Neurolucida software (MBF Bioscience) [28].

After P0 cystograms, the lower bodies of subsets of non-refluxing controls and refluxing mutants were fixed in 4% paraformaldehyde overnight at 4°C and embedded in paraffin for 3D reconstructions [29]. Bladders and ureters were serially sectioned at 6 μm and H&E stained. Bladder and ureter layers were traced in serial sections using a Zeiss Stereomicroscope and captured with a Zeiss AxioCam MRc camera and Stereo Investigator software. From these serial tracings, 3D images were constructed with Stereo Investigator. Neurolucida software was used to trace the ureteral path from its insertion into the bladder wall (external) to the bladder orifice (internal) to calculate the intravesicular tunnel lengths. Neurolucida software was used to construct triangles connecting the bladder wall ureteral insertion sites with the midpoint of the proximal bladder neck (external trigones) and

connecting the ureteral orifices in the bladder lumen to the midpoint of the proximal bladder neck (internal triangles). Neurolucida Explorer was used to calculate external and internal trigone side lengths.

Cystograms

Cystograms were performed on P0 mice to evaluate for VUR [13]. Stillbirths were excluded from cystogram analysis due to concerns for reliability. After euthanasia, the bladder, ureters, and kidneys were exposed. A 60 mL syringe filled with 1% methylene blue in PBS was connected via tubing to a 30-gauge needle. The needle was inserted into the bladder. The bladder was filled by raising the syringe 30 cm every 5 seconds to a final height of 150 cm above the microscope stage, where the syringe was held for 10 seconds. Presence of dye in the ureters or kidneys was consistent with VUR. VUR was graded with an international grading system immediately upon completion of the cystogram, blinded to genotype [30]. Images of the cystogram were independently reviewed by a second individual in a blinded fashion. ImageJ software was used to measure kidney long axis length [27].

Statistics & Rigor

Fisher's Exact Test, Chi-Square test, one-way ANOVA, or two-tailed *t*-tests were conducted where appropriate to determine statistical significance (p value < 0.05) using GraphPad Prism 7 Software (GraphPad Software, La Jolla, CA). For studies that involved phenotypic comparison between mutant and control, genotype was blinded during observations or measurements.

Results

Conditional deletion of *Dicer* from the peri-Wolffian duct stroma

We generated $Tbx18Cre^{Tg/+}$;$Dicer^{flx/flx}$ mice to conditionally delete *Dicer* activity in the peri-Wolffian duct stroma, which should result in loss of mature miRNAs in this tissue. To determine efficiency and specificity of deletion, we dissected E10.5 urogenital ridges and extracted RNA for qPCR; we observed approximately a 50% reduction in mutant *Dicer* exon 24 expression vs controls (0.42±0.06 vs. 1.03±0.16, $p<0.05$) but no changes in mutant *Dicer* exon 21 expression vs controls (0.92±0.10 vs. 1.00±.18 $p=0.71$), which is expected since the former is in the deleted region and the latter is not (Fig 1A) [24]. To confirm expression of active Tbx18Cre allele in the peri-Wolffian duct stroma at the time of ureteric bud induction (E10.5), we examined tdTomato expression in E10.5 $Tbx18Cre^{Tg/+}$*CAG* mice [23, 25]. Whole mount images confirmed active Cre (tdTomato) expression in the peri-Wolffian duct stroma at E10.5 (Fig 1B, C), consistent with prior studies [12, 23]. Prior studies additionally showed Tbx18Cre expression outside of the urinary system, in the pharyngeal area, posterior somites, and epicardium, at E9.5 [23]. Together, $Tbx18Cre^{Tg/+}$;$Dicer^{flx/flx}$ mice have efficient deletion of *Dicer* in the peri-Wolffian duct stroma.

Loss of miRNAs in the peri-Wolffian duct stroma leads to cranially displaced ureteric buds

We then evaluated the site of ureteric bud induction in mutants and controls by performing whole mount calbindin staining at E11.5. Staining revealed that the common nephric ducts (cloaca to the base of the ureteric bud) were often shorter in controls vs. mutants (Fig 2A,

B). We quantified the common nephric duct lengths and the mean control lengths were shorter than the mutants (204.1±10.91 μm vs. 249.4±10.28 μm, respectively, $p< 0.01$) (Fig 2C), consistent with cranial displacement of ureteric bud induction in mutants. For rigor, we also measured E11.5 common nephric duct lengths by 3D reconstructions and confirmed that they were longer in mutants vs. controls, consistent with cranial displacement in the mutants (272.2±16.41 μm vs. 176.2±11.31 μm, $p< 0.001$) (Fig 2D-F). Since generated 3D images do not represent the true physical common nephric duct length, this likely accounts for the difference in the average common nephric duct lengths between whole mount and 3D reconstruction methods. We saw that some ureteric buds were positioned similarly to mutants; however, we did not observe any caudally displaced ureteric buds in the mutants. We observed no duplicate or absent ureteric buds in mutants or controls.

We next examined whether expression of genes known to regulate ureteric induction were altered in mutants vs. controls in E10.5 urogenital ridges by qPCR. Urogenital ridge tissue dissection included the peri-Wolffian duct stroma, ureteric bud, developing gonads, part of the Wolffian duct, and part of the metanephric mesenchyme. We found no differences in mRNA levels of *Gdnf*, *Bmp4*, *Fgfr2*, *Gremlin 1*, *Foxc1* or *Foxc2*, genes expressed in the peri-Wolffian duct stroma [8, 10, 11], in mutants vs. controls (Supplementary Fig 1, Fig S1). We also found no differences in expression of *Pax2* or *Ret*, which are expressed in the ureteric bud and Wolffian duct [13, 14]. Thus, we detected no differences in expression of genes known to regulate ureteric induction in mutants vs. controls to explain the cranial displacement of mutant ureteric buds.

Cranially displaced ureteric buds in mutants are not a result of abnormal metanephric mesenchyme position or delayed CND apoptosis

One possible explanation for a cranial ureteric bud induction is that the metanephric mesenchyme (source of ureteric bud inductive signals) is also cranially shifted in the mutants. To determine whether the position of the metanephric mesenchyme was displaced, we performed histological assessments and 3D reconstructions on E11.5 lower urinary tracts. Histologically, we observed no overt morphological differences in the metanephric mesenchyme in mutants compared to controls, and the proximity of the metanephric mesenchyme to the Wolffian duct and ureteric bud appeared similar (Fig 3A-B, D-E). 3D reconstructions revealed no difference in the positions of the metanephric mesenchyme relative to a plane along the caudal aspect of the hindlimb buds (Fig 3C, F, G). Reconstructions also showed no differences in the long axis lengths or volumes of the metanephric mesenchyme in mutants versus controls (Fig 3H, I).

To determine if abnormal/delayed apoptosis was responsible for the longer mutant common nephric ducts, we performed whole mount E11.5 lower urinary tract co-immunostaining for cleaved caspase-3 and Calbindin (to identify the Wolffian duct, ureteric bud, and common nephric duct). We observed the expected location of apoptosis in the common nephric ducts of both control (Figure 4A-C) and mutants (Figure 4D-F). To determine whether the common nephric ducts met the cloaca and had proper apoptosis patterns, we then performed serial sections immunostained for E-cadherin (to identify the common nephric duct and cloaca) and cleaved caspase-3. The common nephric duct reached the cloaca and apoptosis

was present in the lumen and in cells at the base of the common nephric duct at the cloaca in all control and mutant embryos (Fig 4G-L). Together, abnormal position of the metanephric mesenchyme or abnormal apoptosis do not account for the cranially displaced ureteric buds observed in the mutant mice.

Mice with loss of miRNAs in the peri-Wolffian duct stroma have increased rates of vesicoureteral reflux

Since displaced ureteric buds have been linked to VUR in other models, we next evaluated for VUR. *Tbx18Cre*$^{Tg/+}$*;Dicer*$^{flx/flx}$ mutant mice, although born at expected Mendelian ratio, were perinatal lethal by P1, likely from cardiac or adrenal abnormalities as there is also deletion of *Dicer* in those tissues. We were able to recover 60% of the P0 mutant mice that were not stillbirths to perform cystograms to determine if the aberrant ureteric bud induction led to increased rates of VUR (Fig 5A,B). Mutant mice had significantly increased rates of VUR (8/18) compared to controls (3/77) (Table 1). Most of the mutant mice (7/8) had unilateral VUR. Male mutants trended to have higher rates of VUR (56%) compared to female mutants (33%) (p =0.64, Fisher's Exact test). The grade of VUR trended to be higher in mutant mice compared to controls (p=0.06, Fisher's Exact test), with 62% of mutants having grade II or higher VUR, while all control mice had grade I VUR. Two mutant mice (and no controls) had evidence of hydronephrosis - one unilateral with the opposite side showing VUR and one bilateral (consistent with high-grade VUR). Neither mutant or control mice had renal aplasia, duplex collecting systems, or duplicate ureters. Bladder and ureter morphology appeared similar between mutant and control (Fig 5C,D), including muscle-specific immunostaining with alpha smooth muscle actin (Fig 5E-H), suggesting proper smooth muscle differentiation and patterning. Thus, P0 mice with deletion of miRNAs in the peri-Wolffian duct stroma have significantly higher rates of VUR compared with controls.

Mutant mice have abnormal VUJs on the side of vesicoureteral reflux

To determine whether the VUJs on the side of reflux were abnormal, we performed 3-D reconstructions of subsets of P0 mutant mice with VUR and controls without VUR. First, we noted that refluxing mutant VUJs often had ureters that inserted lower into the bladder wall (3/5) compared with non-refluxing mutant (0/3) or control VUJs (0/6) (Fig 6A-B). Moreover, when we generated triangles to show the external trigones (connecting the external ureteral insertion sites to the bladder neck), we noted a trend for a shorter distance between the ureter insertion site and bladder neck on the side of VUR (Fig 6C-E). 3D reconstructions also revealed that the intravesicular tunnels (portion of the ureter traversing the bladder wall) were significantly shorter in refluxing mutant VUJs than non-refluxing mutant or control VUJs (Fig 6C, D, F). Thus, deletion of miRNAs in the peri-Wolffian duct stroma leads to abnormal formation of the VUJ, characterized by low ureter insertion into the bladder and shortened intravesicular tunnel lengths.

Discussion

In this study, we generated a transgenic mouse model with loss of *Dicer* in the peri-Wolffian duct stroma. This resulted in cranially displaced ureteric bud induction sites. This was not

due to abnormal metanephric mesenchyme, delayed common nephric duct apoptosis, or differential expression of genes known to be important in constraining ureteric bud induction. The ureters tended to insert lower and had shorter intravesicular tunnel lengths in mutant mice with VUR compared to controls. Together, these data show that miRNAs are required to constrain normal ureteric bud position to allow for subsequent normal VUJ formation and prevention of VUR.

Cranial displacement of the ureteric bud could be related to abnormal expression of signaling factors known to constrain ureteric bud induction site, cranial positioning of the metanephric mesenchyme to induce ureteric buds, or delayed apoptosis of the common nephric duct. The latter two defects were not apparent in our model, suggesting that miRNAs in the peri-Wolffian duct stroma either directly or indirectly modify expression of genes that regulate ureteric bud induction. We profiled many of these known genes and found no differences in expression between mutants and controls in whole urogenital ridges at E10.5 during ureteric bud induction. Thus, a strong possibility is that there remains an unknown direct or indirect target of miRNAs from the peri-Wolffian duct stroma that regulates induction. Another possibility is that the cranial-caudal expression pattern or gradient of known factors are altered.

The mutant ureteric buds were either in a normal or cranial position compared to controls, but never in a caudal position. This suggests that miRNAs normally play a role in cranial restraint of ureteric bud position, but do not mediate caudal restraint. The fact that some mutants had normally positioned ureteric buds indicates that other regulators of ureteric bud position can overcome the loss of miRNAs in some cases. Similarly, not all mutants exhibited VUR at P0. Based on the E10.5 qPCR data, Dicer exon 24 reduction varied from 28% to 58% reduction (average, 42%). Thus, there may be a threshold of miRNA expression which is required to prevent abnormal ureteric bud induction and VUR.

Single nucleotide polymorphisms or differential expression of select miRNAs (*hsa-miR-144, hsa-miR-99a-5p*) have been identified in individual patients with VUR [20, 22]. Copy number variations in miRNAs (*miR-125a-5p, let-7e-5p, and miR-126a-3p*) were identified in multiple, unrelated children with VUR who participated in a large cohort study, Randomized Intervention for Children with Vesicoureteral Reflux (RIVUR) [21]. The miRNAs associated with human VUR may be the specific miRNAs that mediate the ureteric bud induction defects that we observed in our mutants.

The abnormal VUJs observed in some of our mutant mice with VUR may be due to (1) abnormal ureteric bud induction sites, as high ureteric bud induction is associated with low ureter insertion [5], or (2) a defect later in embryonic ureter development. Ureter and bladder muscle layers appeared morphologically similar between mutants and controls at P0, so abnormal differentiation is unlikely. Persistence of the common nephric duct at later embryonic time points is also less likely, since this abnormality led to ureter insertion into genital structures or megaureter in other studies [31, 32]. None of these abnormalities were observed in our model, which is consistent with the apparently normal common nephric duct apoptosis patterns we observed at E11.5. We also cannot exclude differences in gene

expression at later embryonic time points after ureteric bud induction that may contribute to abnormal ureter insertion by a yet unknown mechanism.

Shortened intravesicular tunnel length has been associated with VUR in various mouse models [12, 28, 33] and in humans [5]. Mouse models of *Dicer* deletion in the ureteric bud epithelium demonstrate VUJ abnormalities with marked obstructive hydronephrosis and ureteropelvic junction obstruction [34, 35]; however, we rarely observed hydronephrosis (except in the context of high grade VUR) and never observed ureteropelvic junction obstruction in our model. This suggests that miRNAs within the peri-Wolffian duct stroma regulate molecular mechanisms specific to VUR, distinct from miRNAs in the ureteric bud.

In summary, deletion of *Dicer*, and thus miRNAs, in the peri-Wolffian duct stroma led to higher rates of VUR, more cranially displaced ureteric buds, and shortened intravesicular tunnel length on the side of VUR in mutants compared to controls. Thus, these studies demonstrate for the first time that miRNAs in the peri-Wolffian duct stroma regulate molecular mechanisms that suppress vesicoureteral reflux.

Supplementary Material

Refer to Web version on PubMed Central for supplementary material.

Acknowledgements

We thank Feng Chen for the gift of the $Tbx18Cre^{Tg/+}$ mice. MA is supported by NICHD K12 (HD052892) and NIDDK T32 (DK091202-6). JH is supported by DK103776. CB is supported by R01DK104374. SSL is supported by DK096996, DK110503, and DK121758. DMC was supported by a Nephrotic Syndrome Study Network Career Development Award and Children's Hospital of Pittsburgh Research Advisory Council Postdoctoral Fellowship. The work was also supported by the Pittsburgh Center for Kidney Research (P30 DK079307). JH and CB were involved in manuscript draft revisions. All authors contributed to experimental design, data collection, and approved the manuscript prior to submission.

Financial Support: MA is supported by NICHD K12 Grant (HD052892) and NIDDK T32 Grant (DK091202-6). JH is supported by DK103776. CB is supported by R01DK104374. SSL is supported by DK096996, DK110503, and DK121758. DMC was supported by a Nephrotic Syndrome Study Network Career Development Award and Children's Hospital of Pittsburgh Research Advisory Council Postdoctoral Fellowship. The work was also supported by the Pittsburgh Center for Kidney Research (P30 DK079307).

References

1. Chertin B and Puri P, Familial vesicoureteral reflux. J Urol, 2003 169(5): p. 1804–8. [PubMed: 12686848]
2. Murawski IJ *and* Gupta IR, Vesicoureteric reflux and renal malformations: a developmental problem. Clin Genet, 2006 69(2): p. 105–17. [PubMed: 16433689]
3. Craig JC, et al., Does treatment of vesicoureteric reflux in childhood prevent end-stage renal disease attributable to reflux nephropathy? Pediatrics, 2000 105(6): p. 1236–41. [PubMed: 10835063]
4. Murawski IJ and Gupta IR, Gene discovery and vesicoureteric reflux. Pediatr Nephrol, 2008 23(7): p. 1021–7. [PubMed: 18253765]
5. Mackie GG *and* Stephens FD, Duplex Kidneys: A Correlation of Renal Dysplasia with Position of the Ureteral Orifice. The Journal of Urology, 1975 114(2): p. 274–280. [PubMed: 1171997]
6. Costantini F *and* Kopan R, Patterning a Complex Organ: Branching Morphogenesis and Nephron Segmentation in Kidney Development. Developmental Cell, 2010 18(5): p. 698–712. [PubMed: 20493806]

7. Mendelsohn C, Using mouse models to understand normal and abnormal urogenital tract development. Organogenesis, 2009 5(1): p. 306–14. [PubMed: 19568352]
8. Michos O, et al., Reduction of BMP4 activity by gremlin 1 enables ureteric bud outgrowth and GDNF/WNT11 feedback signalling during kidney branching morphogenesis. Development, 2007 134(13): p. 2397–405. [PubMed: 17522159]
9. Sainio K, et al., Glial-cell-line-derived neurotrophic factor is required for bud initiation from ureteric epithelium. Development, 1997 124(20): p. 4077–87. [PubMed: 9374404]
10. Miyazaki Y, et al., Bone morphogenetic protein 4 regulates the budding site and elongation of the mouse ureter. J Clin Invest, 2000 105(7): p. 863–73. [PubMed: 10749566]
11. Kume T, Deng K, and Hogan BL, Murine forkhead/winged helix genes Foxc1 (Mf1) and Foxc2 (Mfh1) are required for the early organogenesis of the kidney and urinary tract. Development, 2000 127(7): p. 1387–95. [PubMed: 10704385]
12. Walker KA, et al., Correction: Deletion of Fibroblast Growth Factor Receptor 2 from the Peri-Wolffian Duct Stroma Leads to Ureteric Induction Abnormalities and Vesicoureteral Reflux. PLoS One, 2016 11(11): p. e0167191. [PubMed: 27861580]
13. Yu OH, et al., Overexpression of RET leads to vesicoureteric reflux in mice. Am J Physiol Renal Physiol, 2004 287(6): p. F1123–30. [PubMed: 15328070]
14. Murawski IJ, et al., Vesico-ureteric reflux and urinary tract development in the Pax2 1Neu+/− mouse. Am J Physiol Renal Physiol, 2007 293(5): p. F1736–45. [PubMed: 17881463]
15. Cordell HJ, et al., Whole-genome linkage and association scan in primary, nonsyndromic vesicoureteric reflux. J Am Soc Nephrol, 2010 21(1): p. 113–23. [PubMed: 19959718]
16. Kelly H, et al., A genome-wide scan for genes involved in primary vesicoureteric reflux. J Med Genet, 2007 44(11): p. 710–7. [PubMed: 17660461]
17. Hwang DY, et al., Mutations in 12 known dominant disease-causing genes clarify many congenital anomalies of the kidney and urinary tract. Kidney Int, 2014 85(6): p. 1429–33. [PubMed: 24429398]
18. Weber S, et al., SIX2 and BMP4 mutations associate with anomalous kidney development. J Am Soc Nephrol, 2008 19(5): p. 891–903. [PubMed: 18305125]
19. Carthew RW and Sontheimer EJ, Origins and Mechanisms of miRNAs and siRNAs. Cell, 2009 136(4): p. 642–655. [PubMed: 19239886]
20. Kohl S, et al., Targeted sequencing of 96 renal developmental microRNAs in 1213 individuals from 980 families with congenital anomalies of the kidney and urinary tract. Nephrol Dial Transplant, 2016 31(8): p. 1280–3. [PubMed: 26908769]
21. Liang D, et al., DNA copy number variations in children with vesicoureteral reflux and urinary tract infections. PLoS One, 2019 14(8): p. e0220617. [PubMed: 31404082]
22. Jovanovic I, et al., Transcriptome-wide based identification of miRs in congenital anomalies of the kidney and urinary tract (CAKUT) in children: the significant upregulation of tissue miR-144 expression. J Transl Med, 2016 14(1): p. 193. [PubMed: 27364533]
23. Wang Y, et al., Cre/lox recombination in the lower urinary tract. Genesis, 2009 47(6): p. 409–13. [PubMed: 19415630]
24. Harfe BD, et al., The RNaseIII enzyme Dicer is required for morphogenesis but not patterning of the vertebrate limb. Proc Natl Acad Sci U S A, 2005 102(31): p. 10898–903. [PubMed: 16040801]
25. Madisen L, et al., A robust and high-throughput Cre reporting and characterization system for the whole mouse brain. Nat Neurosci, 2010 13(1): p. 133–40. [PubMed: 20023653]
26. Livak KJ *and* Schmittgen TD, Analysis of relative gene expression data using real-time quantitative PCR and the 2(-Delta Delta C(T)) Method. Methods, 2001 25(4): p. 402–8. [PubMed: 11846609]
27. Schneider CA, Rasband WS, and Eliceiri KW, NIH Image to ImageJ: 25 years of image analysis. Nat Methods, 2012 9(7): p. 671–5. [PubMed: 22930834]
28. Narla D, et al., Loss of peri-Wolffian duct stromal Frs2alpha expression in mice leads to abnormal ureteric bud induction and vesicoureteral reflux. Pediatr Res, 2017 82(6): p. 1022–1029. [PubMed: 29135976]
29. Hains DS, et al., High incidence of vesicoureteral reflux in mice with Fgfr2 deletion in kidney mesenchyma. J Urol, 2010 183(5): p. 2077–84. [PubMed: 20303521]

30. Lebowitz RL, et al., International system of radiographic grading of vesicoureteric reflux. International Reflux Study in Children. Pediatr Radiol, 1985 15(2): p. 105–9. [PubMed: 3975102]
31. Batourina E, et al., Apoptosis induced by vitamin A signaling is crucial for connecting the ureters to the bladder. Nat Genet, 2005 37(10): p. 1082–9. [PubMed: 16186816]
32. Iizuka-Kogo A, Akiyama T, and Senda T, Decreased apoptosis and persistence of the common nephric duct during the development of an aberrant vesicoureteral junction in Dlg1 gene-targeted mice. Anat Rec (Hoboken), 2013 296(12): p. 1936–42. [PubMed: 24142560]
33. Murawski IJ, et al., The C3H/HeJ inbred mouse is a model of vesico-ureteric reflux with a susceptibility locus on chromosome 12. Kidney Int, 2010 78(3): p. 269–78. [PubMed: 20407478]
34. Bartram MP, et al., Conditional loss of kidney microRNAs results in congenital anomalies of the kidney and urinary tract (CAKUT). J Mol Med (Berl), 2013 91(6): p. 739–48. [PubMed: 23344677]
35. Pastorelli LM, et al., Genetic analyses reveal a requirement for Dicer1 in the mouse urogenital tract. Mamm Genome, 2009 20(3): p. 140–51. [PubMed: 19169742]

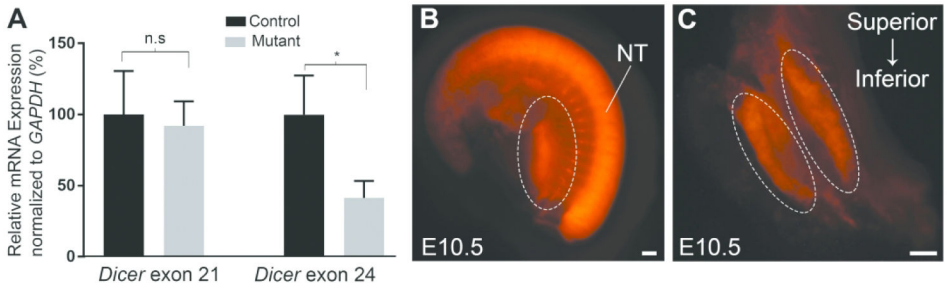

Figure 1. Conditional deletion of Dicer in the peri-Wolffian duct stroma.

(A) *Left*: qPCR shows decreased expression of *Dicer* exon 24 (within the deleted region) in mutant versus control E10.5 dissected urogenital ridge tissue. *Right*: qPCR shows that *Dicer* exon 21 expression (outside of the deleted region) is similar in mutants vs. controls (n = 4 embryos per genotype from 3 litters). All values were normalized to *GAPDH* as a control. (B) Lateral view of an E10.5 embryo from a *Tbx18CreTg/+CAG* mouse shows tdTomato expression (red) in the peri-Wolffian duct stroma (dashed circle) as well as in the neural tube (NT). (C) Ventral view of dissected urogenital ridges demonstrates tdTomato expression in the peri-Wolffian duct stroma at E10.5. Scale bars = 100 μm. Error bars ±SEM. n.s = not significant, * $p<0.05$ vs. control embryos (two-tailed *t*-test).

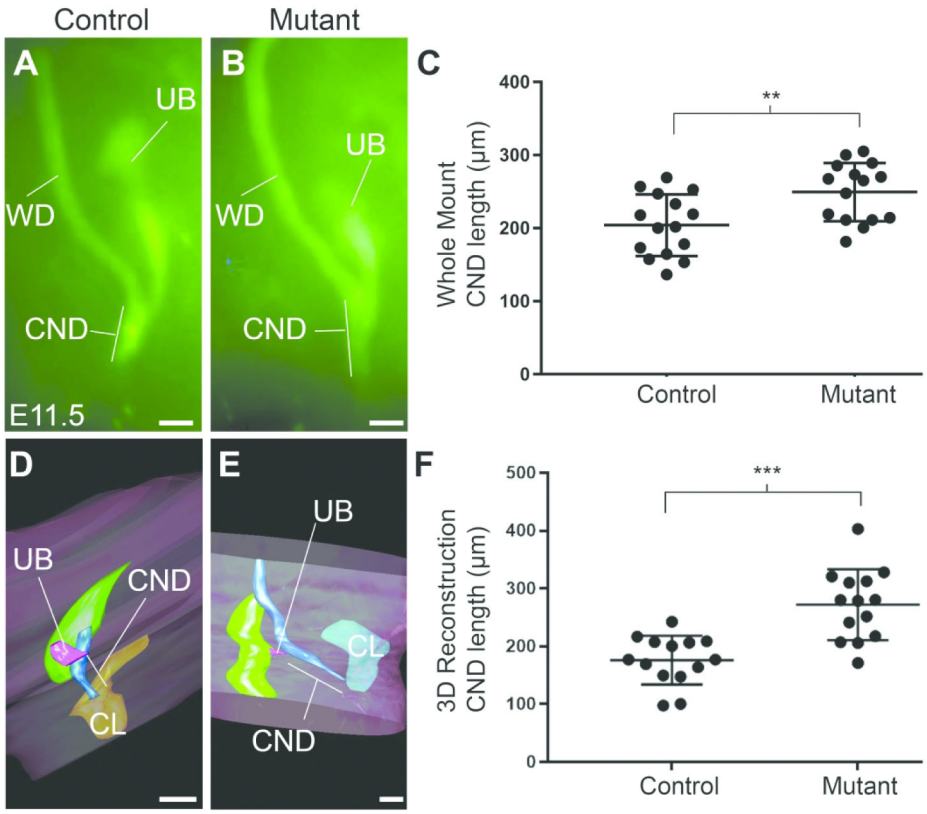

Figure 2. Ureteric bud induction sites are cranially displaced at E11.5.

(A-C) Whole mount Calbindin staining shows a representative control common nephric duct (CND) length (A) that is shorter than the mutant CND length (B), consistent with cranially displaced ureteric buds in the latter. (C) Graph confirms that mean control CND lengths are shorter than mutant lengths (n = 15 common nephric ducts per genotype). (D-E) Representative 3D reconstructions also show a control CND length (D) that is shorter than the mutant (E). (F) Graph showing that mean CND lengths calculated from 3D reconstructions are shorter in controls vs mutants, confirming cranial shifts of the latter. (n = 14 common nephric ducts per genotype). WD = Wolffian duct. UB = ureteric bud. CL = cloaca. Mean = long bar. SD = shorter bars. Scale bars = 100 μm. **p<0.01 and ***p<0.001 (two-tailed *t*-test).

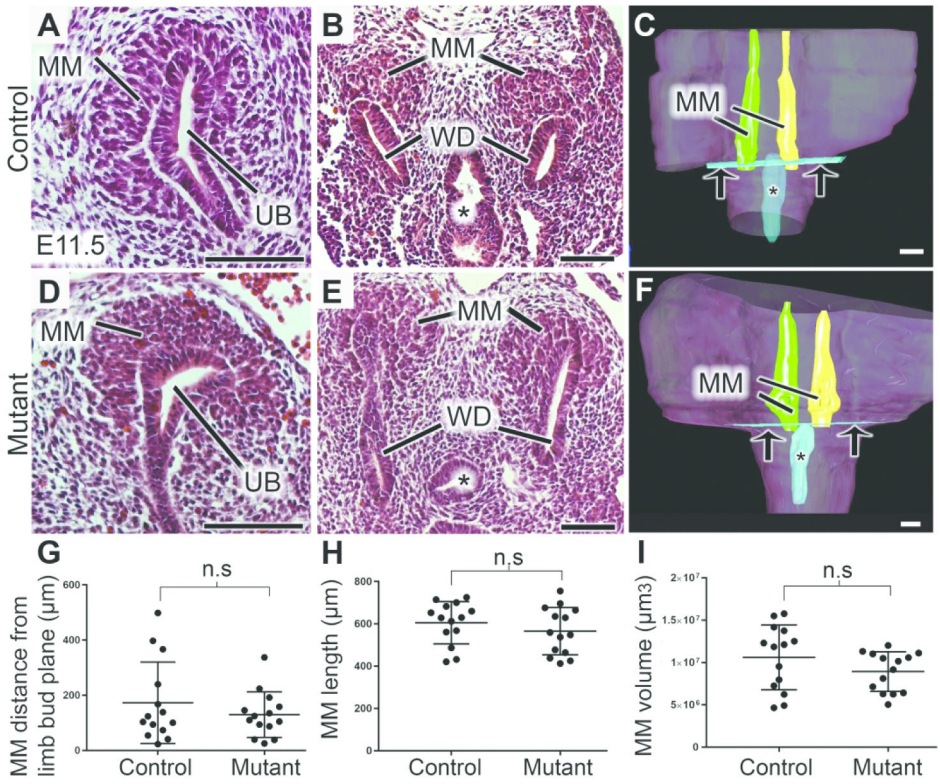

Figure 3. Deletion of miRNAs in the peri-Wolffian duct stroma does not lead to abnormal metanephric mesenchyme position at E11.5.

(A-F) Representative H&E stains show similar metanephric mesenchyme morphology and position relative to the ureteric bud in the control (A, B) and mutant (D, E) E11.5 embryos. Representative images of 3D reconstructions show no apparent differences in positions of the metanephric mesenchyme relative to a plane drawn between the limb buds in E11.5 control (C) and mutant (F) embryos. (G) Graph confirms that the mean distances between the base of the metanephric mesenchyme to a plane at the caudal aspect of the lower limb bud plane were not different between mutant and control E11.5 embryos. (H-I) Graphs show no differences in mean long axis (H) or volume (I) of metanephric mesenchyme between E11.5 controls and mutants. For 3D reconstructions, n = 14 embryos per genotype. MM = metanephric mesenchyme. UB = ureteric bud. * = cloaca. Arrow = limb bud plane. Mean = longer bars. SD = shorter bars. n.s = not significant (two-tailed *t*-test). Scale bars = 100 μm.

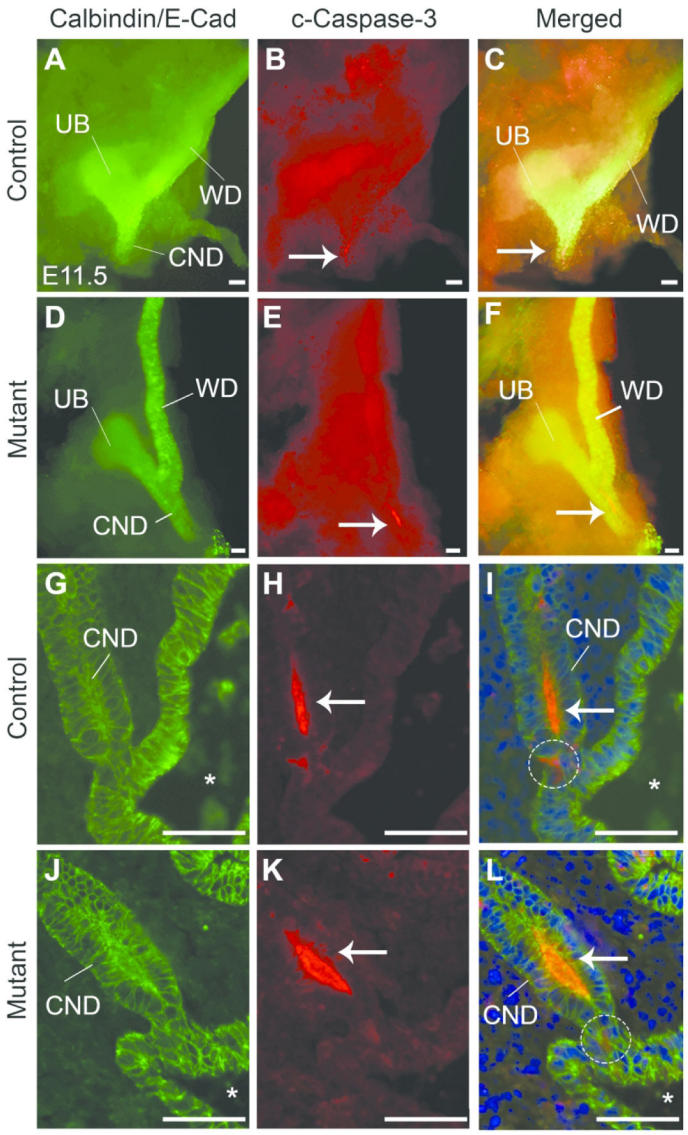

Figure 4. Apoptosis is similar between mutant and control common nephric ducts at E11.5.

(A-F) Whole mount immunostaining for calbindin (A, D) and cleaved-caspase 3 (c-Caspase-3, B, E) demonstrates that apoptosis takes place in the common nephric duct (CND) at similar locations in both control (C) and mutant (F) common nephric ducts at E11.5. (G-L) Whole mount immunostaining for E-cadherin (G, J) and c-Caspase-3 (H, K) reveals that the common nephric ducts reach the cloaca in control (G) and mutant (J) embryos and that apoptosis occurs in the common nephric duct lumen (arrow) and in some cells near the base of the common nephric duct (dashed circle) at the cloaca in control and mutant embryos without overt differences. WD = Wolffian duct. UB = ureteric bud. * = cloaca. Blue = DAPI. Scale bars = 50 μm.

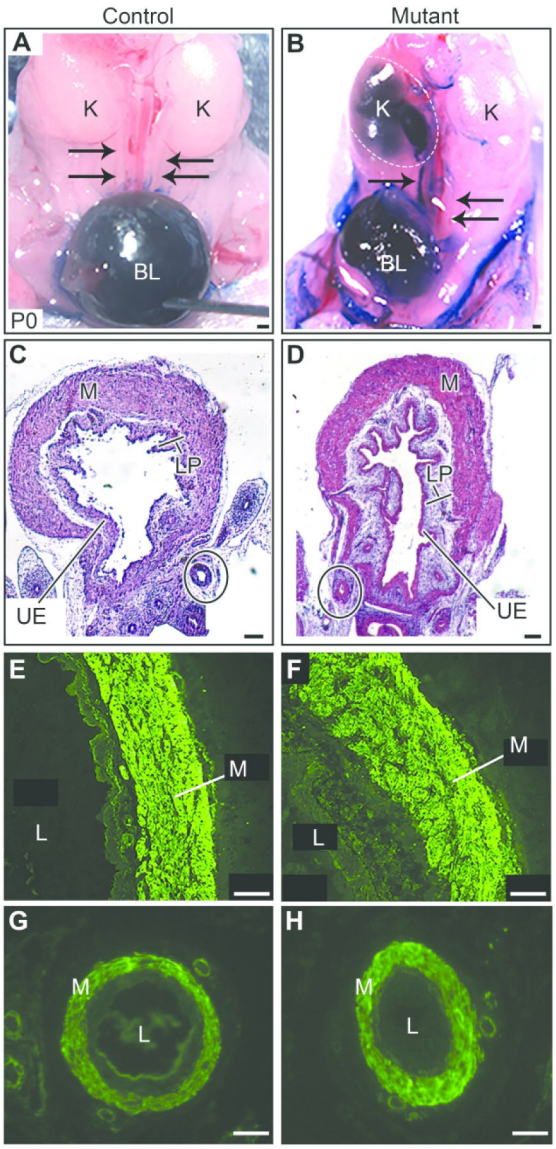

Figure 5. Loss of miRNAs in the peri-Wolffian duct stroma leads to vesicoureteral reflux in mutants at P0.

(A) Representative control cystogram shows methylene blue dye in the bladder (BL) and no dye in the ureters (arrows), consistent with no reflux. (B) Representative mutant cystogram shows no dye in the left ureter (arrows), but significant backflow of dye into the right ureter (arrow) with dilated ureter and dilated right kidney pelvis (K) (dashed oval), consistent with right grade V VUR. (C, D) Representative H&E stains show similar bladder muscle (M), lamina propria (LP), and uroepithelium (UE) in control (C) and mutant (D). Ureters (solid oval) also have intact layers in control and mutant. (E-H) Immunostaining for alpha smooth muscle actin appears similar in control (E) compared to mutant (F) bladder muscle and in control (G) compared to mutant (H) ureter muscle. L = lumen. Scale bars for A-D = 100 μm, E-H = 10 μm.

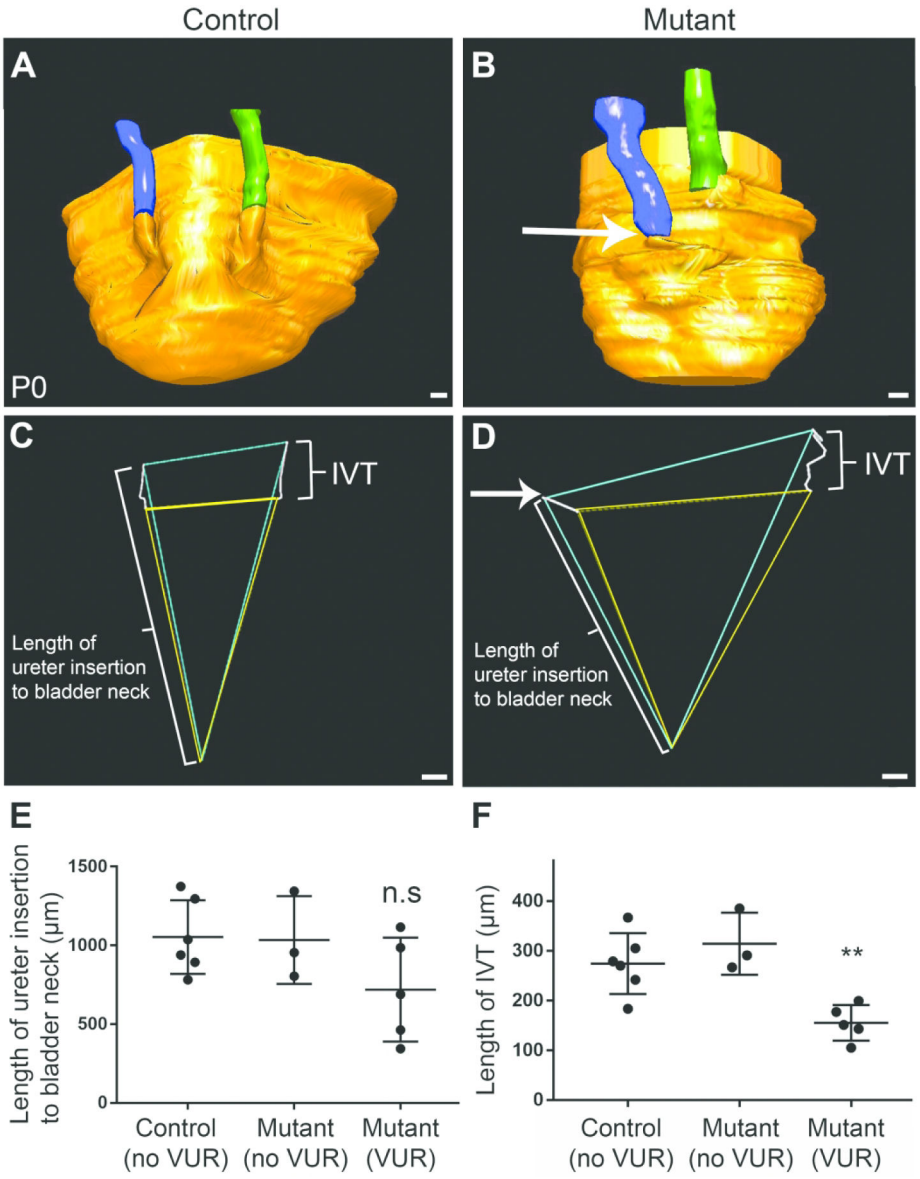

Figure 6. P0 mutant VUJs have low ureter insertions into the bladder and shortened intravesicular tunnel lengths on the side of vesicoureteral reflux.

(A) 3D reconstructions show that ureters insert into the bladder at similar positions in non-refluxing control mice. (B) 3D reconstruction from a mutant with unilateral reflux shows that the refluxing right ureter (arrow) inserts lower into the bladder wall compared to the non-refluxing left ureter. (C, D) Representative external trigones (blue), connecting the external ureter insertion points to the bladder neck and internal trigones (yellow) connecting internal ureter orifice sites to the bladder neck generated from the 3D reconstructions above (A, B respectively). The mutant external trigone demonstrates that the refluxing ureter inserts lower than the non-refluxing ureter (arrow). (E) Graph shows that the mean lengths of the ureter insertion into the bladder wall from the bladder neck (external trigone, indicated with long bracket in C, D) tends to be shorter in mutant VUJs with vesicoureteral reflux compared to non-refluxing mutant or control VUJs (p=0.15). (F) Graph shows that

mean intravesicular tunnel (IVT) lengths (White lines connecting external and internal ureter sites represent the IVT (short bracket) traversing the bladder wall in C, D) are shorter in mutant VUJs on the side of reflux compared to non-refluxing control and mutant ureters. **p < 0.01 One-way ANOVA analysis of variance. Scale bars = 100 μm.

Table 1.

Incidence of vesicoureteral reflux at P0

Genotype	Incidence of Reflux			Reflux laterality	Reflux Grade	
	Total	Male	Female	Unilateral	I	II-V
Control	3/77 (4%)	0/40 (0%)	3/37 (8%)	2/3 (67%)	3/3 (100%)	0/3 (0%)
Mutant	8/18 (44%) **	5/9 (56%)	3/9 (33%)	7/8 (87%)	3/8 (38%)	5/8 (62%)

** $p < 0.01$